

indicate the structure of the disk. The emission distribution over the disk in most of the known cataclysmic variables is far from being uniform or even symmetric. The interaction between the highly supersonic overflowing secondary star material and the edge of the rotating disk and the mass transfer through the disk lead to an inhomogeneous distribution of emission. A prominent region of enhanced emission, the so-called bright spot is often visible at the rim of the disk where the stream material impacts onto the disk. Recently a group found observational evidence for spiral structures in an outburst accretion disk by means of Doppler tomography: Steeghs et al. (1997) found a two armed structure in the disk of IP Peg during outburst. Emission from the secondary star can also play a role, as detected for example for the H_{α} and H_{β} line of IP Peg during quiescence (Wolf et al. 1998). The knowledge of the distribution of line emission is in addition crucial for the measurement of the radial velocity of the white dwarf, since phase-dependent asymmetries in the emission lines distort measurements of this parameter.

This paper presents phase-resolved studies of EX Dra by analysing the spectra presented in Fiedler et al. (1997) in more detail. Our intention is to locate line emitting sites in the system and to obtain information of the line flux distribution over the disk by means of Doppler tomography. Spectra recorded during both the outburst and the quiescent state showing a series of emission lines allow us to compare Doppler maps of different temperatures and accretion states to reveal details of the accretion mechanism in the system EX Dra.

Sect. 2.1 describes the time-resolved spectroscopic observations of the eclipsing dwarf nova EX Dra taken during the quiescent as well as during the outburst state and the applied reduction algorithm. The flux calibration of the spectra is presented in Sect. 2.3. In Sect. 3 the Doppler velocity profiles are discussed and used to map the emission line regions. It is followed by a discussion of the images, a comparison between the high and the low accretion state and a comparison of the Doppler map of H_{α} with the H_{α} map of EX Dra performed by Billington et al. (1996). In Sect. 4 the results of this paper are summarized.

2. Data acquisition and reduction

2.1. Spectroscopy

The acquisition and reduction of the spectroscopic data has already been discussed by Fiedler et al. (1997). Therefore in the following only a short summary of the spectroscopic data is presented. A set of 137 optical spectra of EX Dra was recorded in an observing run at the Calar Alto 3.5 m telescope with the Cassegrain Twin Spectrograph in 1992. The chosen gratings provided a dispersion of 1.7 Å per pixel in the blue and 1.1 Å per pixel in the red spectral range with a wavelength coverage between 3440 and 5330 Å and 5690 and 6810 Å respectively. During these observations EX Dra was in quiescent state.

An additional sequence of 32 spectra was taken in a second observing run at the Calar Alto 3.5 m telescope in 1993 during which EX Dra was found in (probably an early) outburst state.

The wavelength coverage in the red part of the spectra was extended to longer wavelengths (6200. . .8900 Å) at the cost of the spectral resolution leading to a dispersion of 2.7 Å per pixel in the red part of the spectra. The blue part of the wavelength range (3840. . .5630 Å) was observed with a dispersion of 1.8 Å per pixel.

The exposure times varied between 200 s and 1200 s. Spectra of the spectrophotometric standard stars BD +28°4211 (Stone standard) and Wolf 1346 (Oke standard) were taken.

The spectroscopic data were reduced using the so-called Optimal Spectrum Extraction Algorithm (Horne 1986), taking into account bias-subtraction, flatfield-correction, sky-subtraction and cosmic-ray elimination and performing a wavelength-calibration.

In order to correct for the wavelength-dependent sensitivity of the atmosphere and of the instruments a separate flux calibration was performed (see Sect. 2.3).

2.2. Photometry

Long term photometric observations of EX Dra in the quiescent as well as in the outburst state were performed with the Multichannel-Multicolour Photometer MCCP (Barwig et al. 1987) attached to the 80 cm Wendelstein telescope during the years 1991 to 1996 and to the 2.2 m telescope at Calar Alto observatory in 1992 and 1993. The data were recorded with a time resolution of 2 s and 1 s. The MCCP is a high-speed photometer providing three fiber channels to measure the object, a nearby comparison star and the sky background simultaneously. Atmospheric effects are eliminated using the so-called Standard Reduction Algorithm (Barwig et al. 1987) which subtracts the sky background of each of the five UBVRI colour channels from object and comparison star and divides the object by the comparison star measurements afterwards. The simultaneous observing technique in combination with the reduction algorithm allows to perform photometric measurements even under non-photometric conditions. A detailed journal of the photometric observations from 1991 to 1996 is given by Fiedler et al. (1997). The B and R light curves from these photometric measurements were used for the flux calibration of the spectra (see Sect. 2.3).

2.3. Flux calibration of the spectra

A flux calibration is required in order to account for the wavelength- and time-dependent sensitivity of the atmosphere, for the wavelength-dependent sensitivity of the telescope, the spectrograph and the detector and to transform the recorded flux distribution to an absolute scale.

Under stable atmospheric conditions the flux calibration can be performed by using recorded spectra of spectrophotometric standard stars, or alternatively by using simultaneously recorded broadband photometry. The latter can also be applied under variable atmospheric conditions, when an instrument like the MCCP is used which allows to obtain photometric measurements even under non-photometric conditions.

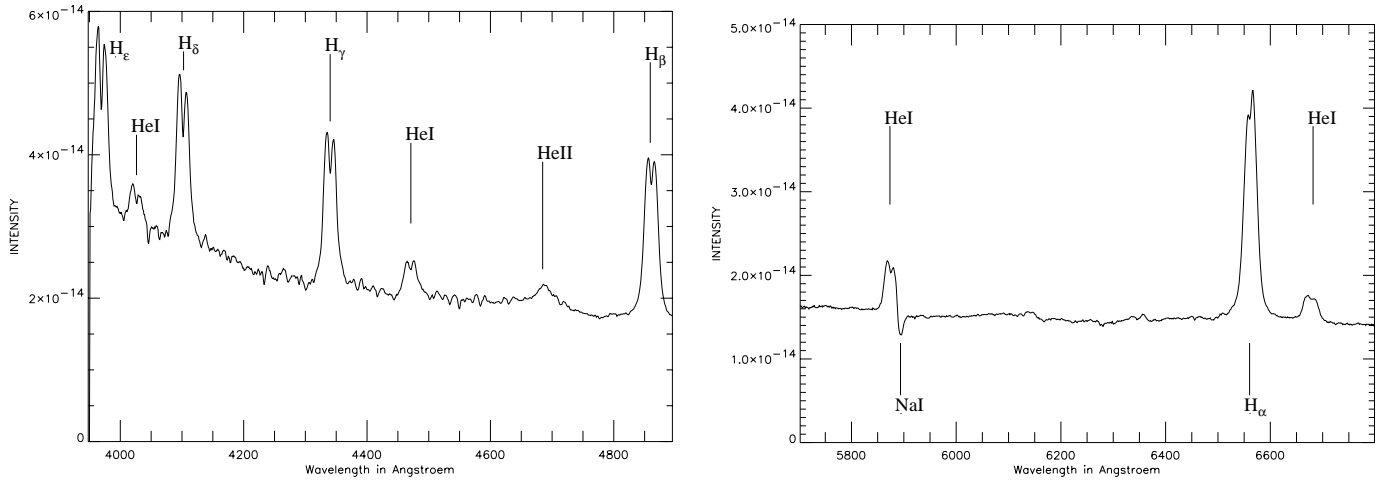


Fig. 1. Mean spectra of EX Dra observed during quiescence. Before averaging the spectra were shifted according to the radial velocity $K_1 \sin(\phi) = 167 \text{ km s}^{-1} \sin(\phi)$. Intensities in $\text{ergs s}^{-1} \text{ cm}^{-2} \text{ \AA}^{-1}$. The energy flux is accurate to a constant factor, because of slit loss of the flux star spectra. See the text for more details.

Unfortunately the atmospheric conditions were not stable during the observations and no simultaneous photometry was available which could have been used to correct for the atmospheric variations. In addition a careful check of the recorded standard star spectra showed that a significant loss of light occurred at the spectrograph slit.

Therefore a different approach had to be made: the short term atmospheric variations were corrected by means of *mean* photometric B and R light curves taken during the quiescent and the outburst states of EX Dra, whereas the wavelength-dependent sensitivity of the atmosphere and the instrument were corrected by using the recorded spectra of the flux stars BD+28°4211 (1992) and Wolf 1346 (1993). A significant number of photons is lost when a narrow spectrograph slit is used for both the object as well as the standard star spectra. The lack of standard star spectra recorded with a wide slit prevented us from calculating the so-called ‘slit loss’. Therefore the resulting spectral flux distribution of the object spectra is accurate to a constant factor.

3. Analysis and results

3.1. Mean quiescence spectra

Fig. 1 presents the mean spectra of EX Dra in quiescence, which are based on 69 single spectra in the blue and 68 in the red wavelength range. Before averaging the single spectra were shifted according to the radial velocity $K_1 \sin(\phi)$, with $K_1 = 167 \text{ km s}^{-1}$ (Fiedler et al. 1997). The spectra show strong, broad emission lines of hydrogen with equivalent widths up to 55 \AA for H_α . Neutral helium is present in emission in both the singlet line at $\lambda 6678 \text{ \AA}$ and the triplet lines at $\lambda\lambda 4471, 4026, 5876 \text{ \AA}$. He II is weakly present at $\lambda 4686 \text{ \AA}$. Lines from other (highly) ionized species are rarely seen during quiescence, except several Fe II ($\lambda\lambda, 4924, 5018, 5169 \text{ \AA}$) lines.

The hydrogen and helium emission lines show the typical double-peaked profiles associated with accretion disks and are

therefore mainly formed within the disk. These profiles are superimposed by asymmetric structures produced by anisotropically radiating emission sites of the system. The Balmer lines $H_\beta, H_\gamma, H_\delta, H_\epsilon$ and the He I ($\lambda 6678 \text{ \AA}$) line show an asymmetry in form of an enhanced *blue-shifted* peak in the averaged spectra. The phase-resolved single spectra of these lines show clearly that the maximum of line emission is seen during the phases before the eclipse ($\phi \approx 0.7 \dots 0.95$) in the blue-shifted part of the line profiles. Obviously it can be attributed to the interaction between the infalling gas stream and the outer parts of the disk which produces an anisotropically radiating region of enhanced emission.

Departing from that canonical picture the line profile of the H_α line shows an asymmetry in form of an enhanced *red-shifted* peak. Obviously at lower temperatures the emission of the bright spot is exceeded by other sources of emission within the system. The phase-resolved line profiles reflect a complex structure indicating that several emission sites contribute to the H_α line flux, but do not allow a separation of the different components. This will be further discussed in Sect. 3.3 in the context of the Doppler maps.

The secondary star is visible in several Ca I absorption lines in the red part of the optical wavelength range. A detailed analysis of these lines can be found in Fiedler et al. (1997).

3.2. Mean outburst spectra

The mean spectra of EX Dra in outburst are displayed in Fig. 2 as the average of 16 single spectra for the blue and 16 for the red spectral range. As discussed in Sect. 2.3 the spectra of the spectrophotometric standard stars suffered from significant slit loss and therefore the computed flux of the spectra of EX Dra is accurate to a constant factor. The energy flux of the system appears to be higher in quiescence than outburst. The mentioned slit loss should account for this contradiction, since we know from photometric measurements taken the night after the spectroscopic

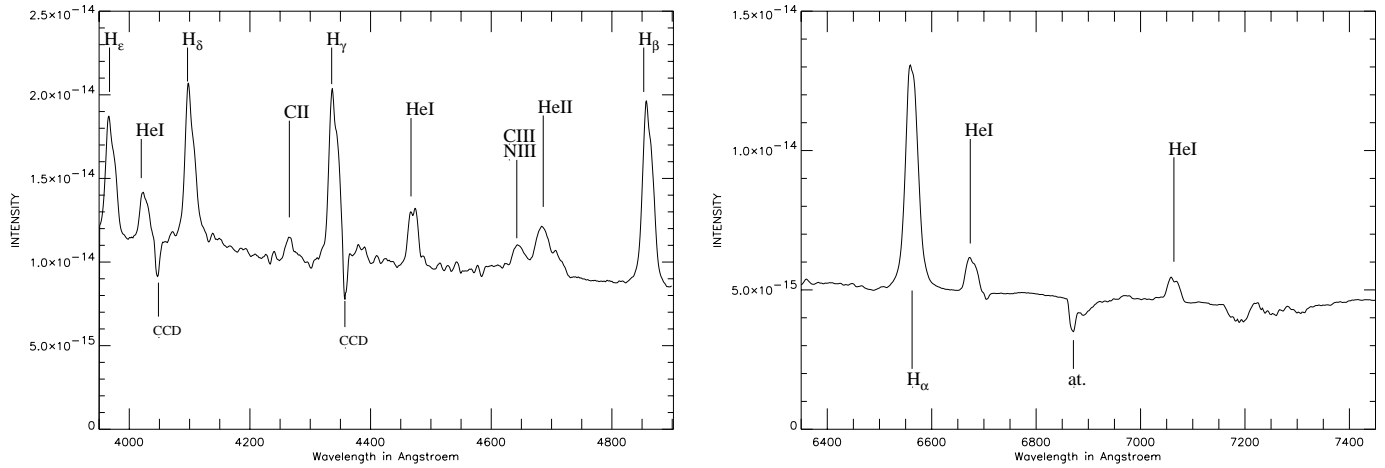


Fig. 2. Mean spectra of EX Dra observed during outburst. Before averaging the spectra were shifted according to the radial velocity $K_1 \sin(\phi) = 167 \text{ km s}^{-1} \sin(\phi)$. Intensities in $\text{ergs s}^{-1} \text{ cm}^{-2} \text{ \AA}^{-1}$. The flux is accurate to a constant factor, because of slit loss of the flux star spectra. This fact could explain why the energy flux of the system appears to be lower during outburst than during quiescence. See the text for further discussion.

observations in 1993 that the optical flux was significantly enhanced compared to July 1992.

The most remarkable features in the outburst spectra are dominant emission lines of the Balmer series and of neutral helium, whereas outburst spectra generally show broad Balmer absorption lines with weak emission cores. A similar behaviour was also seen in IP Peg: Marsh & Horne (1990) recorded outburst spectra of IP Peg and observed enhanced emission line fluxes of all Balmer and helium lines with He II ($\lambda 4686 \text{ \AA}$) becoming the strongest line at visual wavelengths. The systems Z Cha (Vogt 1982) and OY Car (la Dous 1991) also show emission lines during outburst. The high orbital inclination of these systems probably account for the strong emission lines during eruption, because the flux in the optically thick continuum of the accretion disk is at large inclinations reduced by projection and limb darkening in favor of emission lines formed above the disk.

The profiles of the Balmer lines are almost single-peaked in the mean spectra of EX Dra in outburst, although there are still some small indications of double-peaked structures visible. As a remarkable exception the He I ($\lambda 4471 \text{ \AA}$) line clearly displays a double-peaked profile in the mean outburst spectra.

High-excitation lines which are only weakly or not at all present during quiescence emerge during outburst, like He II ($\lambda 4686 \text{ \AA}$), C II ($\lambda 4267 \text{ \AA}$) and the C III/N III ($\lambda\lambda 4634 \dots 4651 \text{ \AA}$) blend.

He II emission is often a hint for a strong magnetic field of the white dwarf, but there is no evidence for magnetic accretion in EX Dra. Patterson & Raymond (1985) show that He II ($\lambda 4686 \text{ \AA}$) emission can be produced in the upper layer of the disk by reprocessing soft X-rays from the boundary layer when the mass transfer rate $\dot{M}(d)$ exceeds $10^{-9} M_{\odot}/y$. Under the premise that $\dot{M}(d)$ in EX Dra in the recorded outburst state satisfies this condition the detected He II outburst line could be formed in the (upper layer of the) disk by recombination following photoionization by the boundary layer. He II is blended

by C III/N III emission, which prevents us from Doppler imaging this line. The time-resolved line profiles show that the line forming region can not be too extended since most of the He II emission is eclipsed at phase $\phi = 0$ by the secondary star.

3.3. Doppler imaging in the quiescent state

Line profiles broadened by Doppler shifting retain an imprint of the line emission region from which it originated. The Doppler tomography is an imaging technique, developed by Marsh & Horne (1988), which makes use of the close relationship between the observed emission line flux and the velocity profiles to obtain the distribution of line emission over the surface of the disk in velocity space.

Under the premise that Doppler shifting is the only broadening mechanism of significance it is possible to locate the line forming regions of the binary system by means of Doppler tomography.

The Doppler broadened line profiles represent a projection of the velocity distribution in the direction of the observer's line of sight, while rotation of the binary gives the observer a continuously varying sequence of velocity projections. This combination of Doppler shifting and binary rotation provides sufficient information for the assembly of two-dimensional maps in velocity space (V_x, V_y).

While the observed line profiles are a projection of the velocity distribution, a back-projection algorithm applied to the observed data yields the emission distribution in velocity space.

The computation of a Doppler tomogram is based upon the fundamental fact, that a spot of emission in the binary system traces an 'S-wave' in the phase-sorted ('phase-folded') spectra, most evidently displayed by the features of the bright spots in many cataclysmic variables. The coordinate system is defined by the X-axis pointing from the white dwarf to the secondary star and the Y-axis in the direction of motion of the secondary star. The sinusoidal 'S-wave' radial velocity curve V_R described

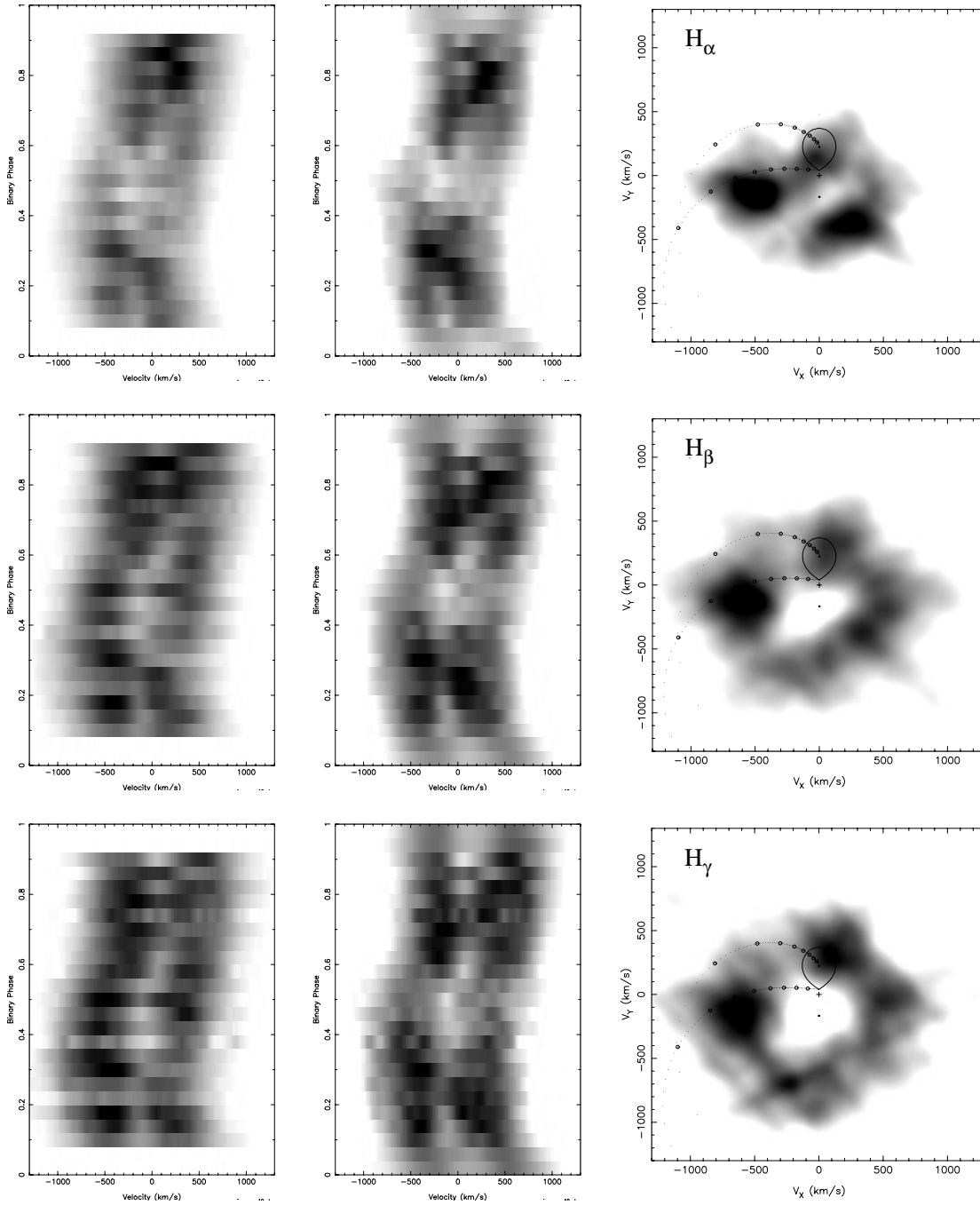


Fig. 3. Doppler maps of H_{α} , H_{β} and H_{γ} during the quiescent state of EX Dra (right column), the observed phase-folded spectra (left column) and the spectra reconstructed from the maps (middle). The Doppler maps show a broad ring-like structure and emission from the gas stream. The map of H_{α} displays further a second bright emission spot at $V_x \approx 0 \dots +500 \text{ km s}^{-1}$ and a faint hint of secondary emission.

Billington et al. (1996) also found evidence for irradiation of the secondary in their H_{α} Doppler map. In contrast to our result they observed strong broadened secondary star emission uniformly distributed over the secondary including L_1 . This might be due to their incomplete phase coverage and fewer number of spectra compared to our data set.

The disk structures in the H_{γ} , H_{δ} and $\text{He I } (\lambda 4471 \text{ \AA})$ maps are superposed by several emission features weaker than the

bright spot. The features in H_{γ} and H_{δ} are consistent. Since such features can be caused by a low phase resolution they might be artificial. Further spectroscopic observations with higher time and velocity resolution are required to verify their existence.

3.4. Doppler imaging in the outburst state

Interpretation of Doppler tomograms of the outburst state is hampered by the fact that the outburst data set covers only 56%

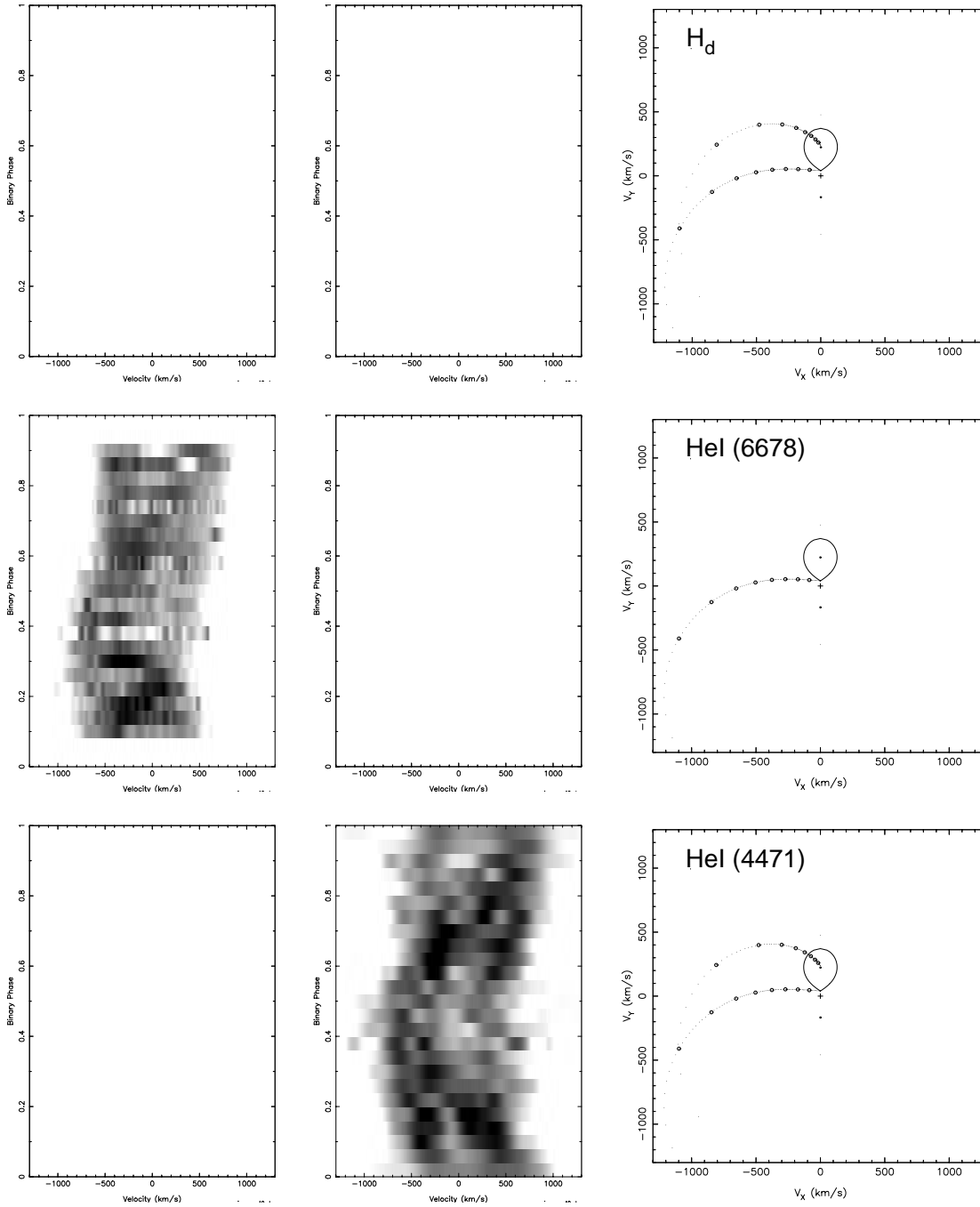


Fig. 4. Doppler maps of H and He I (6678 and 4471) during the quiescent state of EX Dra (right column), the observed phase-folded spectra (left column) and the spectra reconstructed from the maps (middle). The H shows similar features as the H and H map (cp. Fig. 3). The He I maps display emission from the gas stream and the disk, but the data are quite noisy within this lines.

of the binary orbit, which could result in artificial effects. Duplications of He I (6678A) emission from the secondary during to a non uniform distribution of the available spectra across the binary orbit we obtain a decreased resolution in the reconstruction. Because of the mentioned artificial smearing in the direction the bright emission region in the H butburst map can be a

As in many dwarf novae during outburst, EX Dra shows superposition of emission from the irradiated secondary and the strong Balmer emission from the secondary star in the high gas stream. Emission from the gas stream is further detectable in the quiescent state (Fig. 5). The secondary star displays no emission in the He I maps, most prominently in the line at 4471A. A comparison with the He I (4471A) quiescence map locates

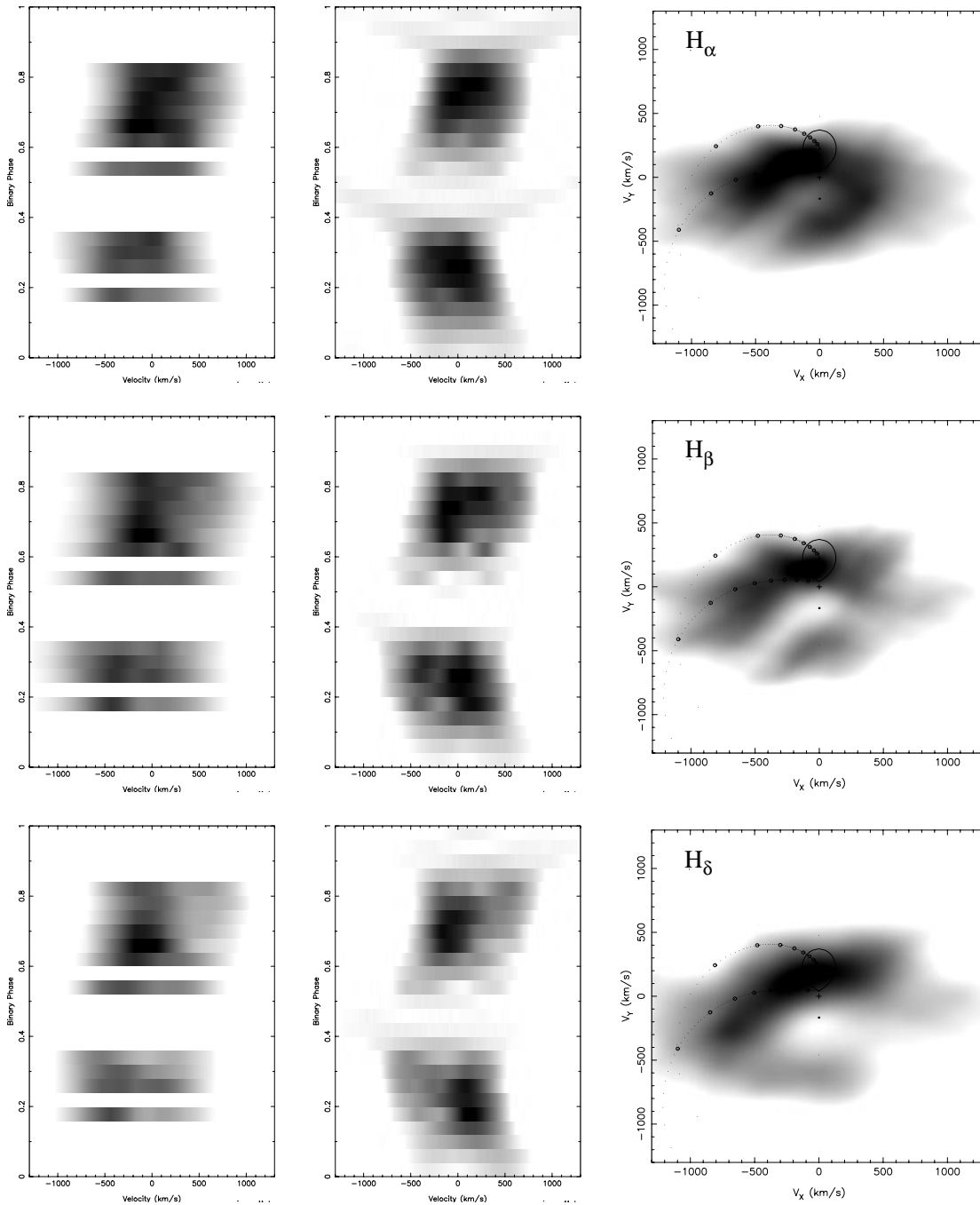


Fig. 5. Doppler maps of H_{α} , H_{β} and H_{δ} during the outburst state of EX Dra (right column), the observed phase-folded spectra (left column) and the spectra reconstructed from the maps (middle). The images show strong secondary star emission. Emission from the gas stream obviously contributes to the bright emission region in the H_{α} map. Due to an incomplete phase coverage of the outburst data set an artificial smearing in the V_x direction occurs.

the impact region in outburst about $0.2 R_{L1}$ closer to the L_1 point than in quiescence. This can be attributed to the enhanced accretion during outburst, which causes an enlargement of the outer disk regions due to conservation of angular momentum within the disk.

The system seen in the light of the single ionized carbon (Fig. 6) differs totally from the other images. The C II emission which is only marginally detectable in quiescence is powerful

enhanced during outburst. The S-wave in the observed phase-folded spectra (lower left picture in Fig. 6) indicates that the C II line flux is emitted at relatively low radial velocities. In the Doppler image the C II emission is concentrated in the center of the disk suggesting a line forming region close to the white dwarf. Whether C II originates in the chromosphere of the primary or in parts of the inner boundary layer or in a wind from the white dwarf is not clear. The reconstructed data (lower mid-

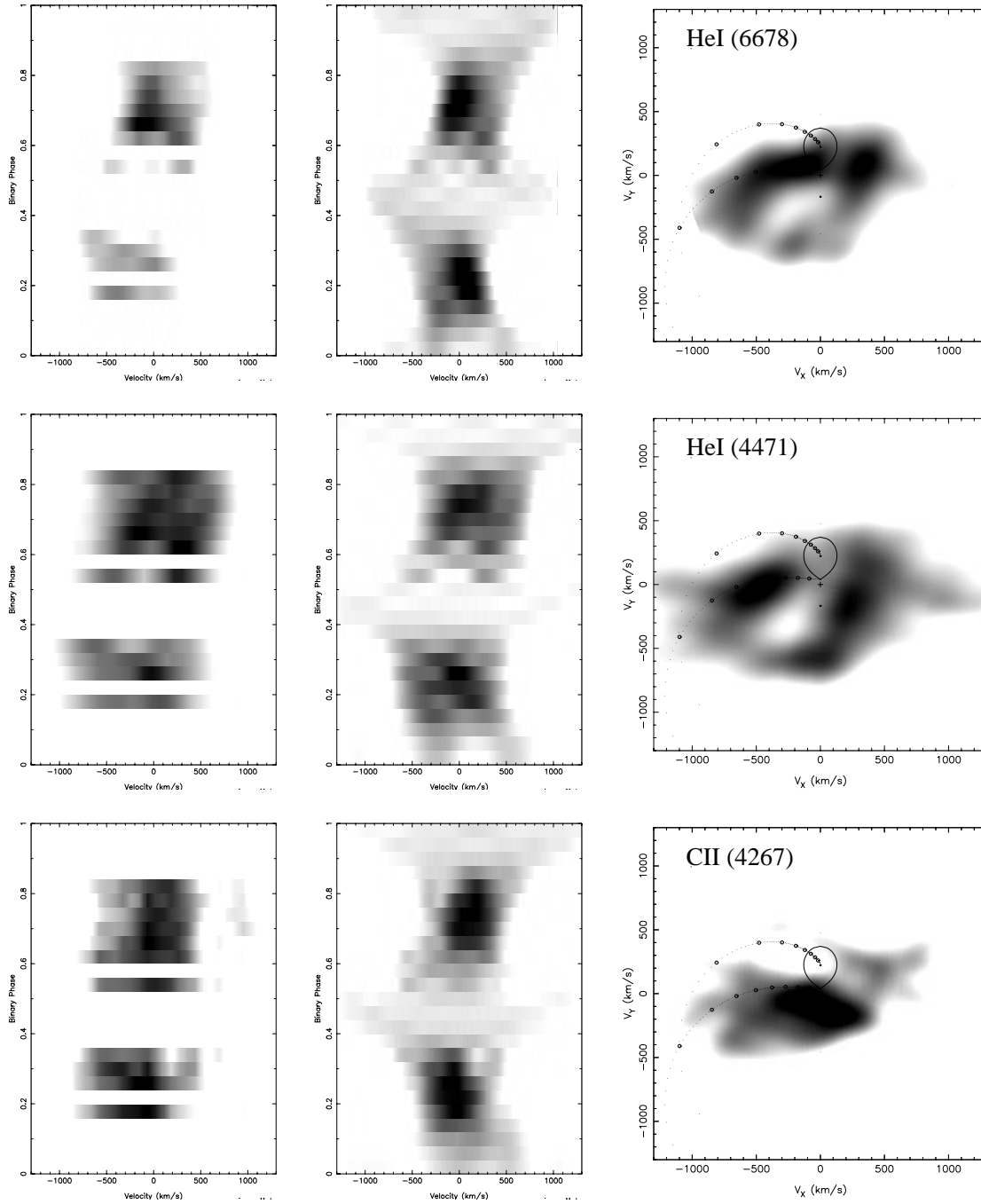


Fig. 6. Doppler maps of He I ($\lambda\lambda$ 6678, 4471 Å) and C II (λ 4267 Å) during the outburst state of EX Dra (right column), the observed phase-folded spectra (left column) and the spectra reconstructed from the maps (middle). In the He I maps there is detectable emission from the gas stream and a further structure almost opposite to this feature. The C II line differs totally from the other lines. A narrow component in the phase-folded data maps into a region in the velocity map close to the primary component.

dle picture in Fig. 6) indicate a reliable back-projection, but the interpretation of the C II line is hampered by the low S/N ratio of the data recorded within this line and by possible artificial effects due to the incomplete phase coverage and the low phase resolution. However, it is obvious that during outburst the C II line is not emitted from the same sites, where the Balmer or helium lines originate.

The two He I outburst maps (cp. Fig. 6) clearly display emission features in the disk almost opposite to the bright spot. Recently detected spiral structures in the outburst accretion disk of IP Peg (Steehns et al. 1997) suggest that tidally induced spiral shocks (first proposed by Sawada et al. 1986, 1987) may also play a role in the accretion processes during outburst in other dwarf novae. Unfortunately the low spectral and phase-resolution of our outburst data permit no reliable statement about

spiral structures in the disk of EX Dra. The detection of spiral patterns by means of Doppler tomography demands a spectral resolution of 80 km s^{-1} and a time resolution of 40 spectra per binary orbit (Steehgs & Stehle 1999), which is not met by our outburst data set.

4. Discussion and conclusion

EX Dra in quiescence is dominated by emission from a fully established accretion disk and by emission from the gas stream interacting with its outer rim. The center of the gas stream emission located at $\sim 500 \text{ km s}^{-1}$ during quiescence is in agreement with that in the Hmap of Billington et al. (1996), but our data set does not confirm the strong broadening detected by Billington et al (1996).

Unlike most other dwarf novae, the emission lines of EX Dra remain strong during outburst. This behaviour is also seen in other deeply eclipsing dwarf novae like IP Peg (Marsh & Horne 1990), Z Cha (Vogt 1982) and OY Car (la Dous 1991). The high orbital inclination of these systems probably accounts for the strong emission lines during eruption, because at large inclinations the flux in the optically thick continuum of the accretion disk is reduced by projection and limb darkening in favor of emission lines formed above the disk.

Reemission of the secondary star in EX Dra is detectable during quiescence in H and during outburst in H β , H γ and H δ , where it becomes the dominating emission source during outburst. The emission is concentrated near the poles of that side of the secondary facing the primary and indicates photospheric heating caused by irradiation by the white dwarf or the boundary layer.

Emission lines from highly excited species, like He I ($\lambda 4686\text{\AA}$), C II ($\lambda 4267\text{\AA}$) and C III / N III ($\lambda 4634\text{\AA} : : 4651\text{\AA}$) are only marginally or not at all detected during quiescence but become strongly enhanced during outburst.

The Doppler image of the C line during outburst locates its line forming region close to the white dwarf. This suggests the chromosphere of the white dwarf or the inner boundary layer or an outflow as possible emission sites. Radial velocity measurements of this line should in principle reproduce the radial velocity of the primary with higher precision than the distorted disk emission lines do. However, due to the low S/N of this C line and the incomplete phase coverage of the recorded outburst spectra, we were not able to determine the radial velocity of the C II line.

The He II line is superimposed by C III / N III emission, for that reason no reliable Doppler map of this line can be formed. Provided that the mass transfer rate exceeds $10^{-9} M_{\odot} \text{ yr}^{-1}$ (Patterson & Raymond 1985) the He emission during outburst might be produced by reprocessing of soft rays from the boundary layer in the disk.

It is further conceivable that He II (and C II) is formed in outflowing material, but this would require a very slow wind. However, the material emitting the He II and C II lines can not be too extended, but must be closely connected to the orbital plane since both emission lines are eclipsed at phase 0.

A comparison between the location of the gas stream emission in the Doppler maps of He I ($\lambda 4471\text{\AA}$) in quiescence and outburst show that the disk radius is enlarged by about $0.2 R_1$ during outburst.

The brightest line forming region in quiescence in the Doppler map of H β is located far from the gas stream trajectory. We have no explanation which line forming processes are involved to produce this feature. Since this emission spot is only detectable in the H line and not in lines reflecting higher temperatures it is unlikely to be caused by a second impact region, as discussed e.g. by Lubow (1989). This emission spot is partly responsible for the complex H line profiles and the asymmetric profile in the averaged spectra in form of an enhanced redshifted peak.

The He I maps computed for the outburst spectra show evidence for emission structures in the right and top right region of the Doppler maps. Unfortunately the quality of the outburst spectra does not allow to draw a clear decision whether these structures may be attributed to spiral structures within the accretion disk of EX Dra, as detected for IP Peg during outburst (Steehgs et al. 1997), or not. Our results show that EX Dra is a very interesting CV and that the next step should be spectroscopy with higher time and spectral resolution. The fact that the system can be frequently found in the outburst state should make further investigation possible throughout its outburst cycle.

Acknowledgements We thank Vadim Burwitz for helpful discussions and useful comments on the manuscript. We also thank C. Ries for collecting photometric data at Wendelstein observatory. Part of this work was supported by the Deutsche Forschungsgemeinschaft grant Ba 867/3-1, Ba 867/5-1.

References

- Barwig H., Schoembs R., Buckenmayer C., 1987, A&A 175, 327
- Barwig H., Fiedler H., Reimers D., Bade N., 1993, In: Compact Stars in Binary Systems, van Woerden H. (ed.) Abstracts of IAU Symp. 165, p. 89
- Billington I., Marsh T.R., Dhillon V.S., 1996, MNRAS 278, 673
- Fiedler H., Barwig H., Mantel K.H., 1997 A&A 327, 173
- Horne K., 1986, PASP 98, 609
- Horne K., 1991, In: Fundamental Properties of Cataclysmic Variable Stars: 12th North American Workshop on Cataclysmic Variables and Low Mass X-ray Binaries, San Diego State University Publication, San Diego, Shafter A.W. (ed.) p. 160
- la Dous C., 1991, A&A 252, 100
- Lubow S.H., 1989, ApJ 340, 1064
- Marsh T.R., Horne K., 1988, MNRAS 235, 269
- Marsh T.R., Horne K., 1990, ApJ 349, 593
- Patterson J., Raymond J.C., 1985, ApJ 292, 550
- Sawada K., Matsuda T., Hachisu I., 1986, MNRAS 219, 75
- Sawada K., Matsuda T., Inoue M., Hachisu I., 1987, MNRAS 224, 307
- Steehgs D., Stehle R., 1999, MNRAS 307, 99
- Steehgs D., Harlaftis E.T., Horne K., 1997, MNRAS 270, L28, Erratum: 1998 MNRAS 296, 463
- Vogt N., 1982, ApJ 252, 563
- Wolf S., Barwig H., Bobinger A., Mantel K.H., Simic D., 1998, A&A 332, 984